Supporting Information

Electrode|Electrolyte Interface Enhancement in Quasi-Solid-State Zinc-Air Batteries through Anion Conducting Polymer Electrolyte Interlayer by *in-situ* Polymerization

Maria Kurian,[a.b] Vidyanand Vijayakumar,[a] Narugopal Manna,[a,b] Fayis Kanheerampockil,[a,c] Suresh Bhat,[a,c] and Sreekumar Kurungot*[a,b]

[a] Maria Kurian, Vidyanand Vijayakumar, Narugopal Manna, and Sreekumar Kurungot*
Physical and Materials Chemistry Division, CSIR-National Chemical Laboratory, Pune, 411008, India. Maharashtra, India. E-mail: k.sreekumar@ncl.res.in

[b] Maria Kurian, Narugopal Manna, Fayis Kanheerampockil, Suresh Bhat, and Sreekumar Kurungot*
Academy of Scientific and Innovative Research, Postal Staff College Area, Kamla Nehru Nagar, Ghaziabad, Uttar Pradesh-201002.

[c] Fayis Kanheerampockil and Suresh Bhat

Polymer Science and Engineering Division, CSIR-National Chemical Laboratory, Pune, 411008, India.

Experimental details:

1. Physical Characterization:

The structural features of the prepared polymer membrane and materials were evaluated using Fourier Transform Infrared (FTIR), and Field Emission Scanning Electron Microscopy (FESEM). Attenuated Total Reflection (ATR) spectrometer Spectrum GX (Perkin Elmer, Waltham, MA) was used to record the FTIR spectra of the precursor solution and AEPEM-GF polymer membranes in the infrared range of 4000-400 cm^{-1}. Universal Testing Machine (UTM) (Model: Instron 5943, Instron Ltd., MA, USA), was used to study the mechanical stability of the polymer electrolytes equipped with 1 kN load cell and a constant crosshead speed of 5 mm min^{-1}. For this purpose, the strips of polymer membrane of dimension 0.5 cm x 3 cm were prepared. The samples were stretched laterally until fractured. The tensile stress and strain were recorded, calculated, and plotted for every sample.

The Confocal Laser Scanning microscope (CLSM) (Zeiss, Oberkochen, Germany Model LSM 710) is used for background-free high-resolution images of AHM-skin-integrated Pt/C-RuO_2-coated

air-electrode. The instrument has an EC Epiplan-APOCHROMAT objective of 50X magnification and a numerical aperture of 0.9. Fluorescence from the sample was excited with the 543 nm line of a He-Ne laser. The bandpass sliders (625 -641 nm) in front of the spectral detectors separated the fluorescence from the excitation light. To procure three-dimensional images, the microscope objective was attached to an opto-electronically coded focus z-driver to scan along the vertical z direction. A pinhole is used to reject the out-of-plane light for background rejection to obtain a better signal-to-noise ratio. Around 30-50 sliced stacks of 512 X 512-pixel images were acquired in the horizontal x–y plain separated by 1 um in the z-direction. The full-sized field of view length is approximately 170 µm and a depth of approximately 10 µm, and for the cross-section images, the full-sized field of view is approximately 625 µm and a depth of approximately 10 µm . The images were processed using the Zen software (Zeiss, Oberkochen).

2. Electrochemical Characterization:

The Biologic-VMP3 instrument was used to perform the half-cell studies of the catalyst developed and ZAB full-cell analysis. The ionic conductivity of the AEPEM and AEPEM-GF membranes was determined by Electrochemical Impedance Spectroscopy (EIS). The membranes of 1.34 cm^2 area were sandwiched between two stainless steel plates in a CR2032-coin cell assembly inside an ESPEC SH-241 climatic chamber for temperature dependant conductivity measurements. The impedance measurements were carried out in the temperature range of 20°C and 60°C, at every 10°C intervals by maintaining the temperature equilibrium and in the frequency range of 1 MHz to 1 Hz, at open-circuit voltage (OCV). The ionic conductivity (σ, S cm^{-1}) was measured using Equation S1, where 'R' is the bulk resistance, 'l' is the thickness, and 'A' is the area of the sample.

$$\sigma = l/A\,R \qquad \textbf{Equation S1}$$

3. Material preparation and device fabrication.

Preparation of AEPEM and AEPEM-GF:

For the preparation of the AEPEM, a reactive solution (also called the precursor solution) consisting of the monomers/oligomers *viz;* 2-(acryloyloxy)ethyltrimethylammonium chloride solution (AOETMA), (hydroxyethyl) methacrylate (HEMA), poly(ethylene glycol) methyl ether methacrylate (PEGMEMA) were taken in appropriate concentrations as given in **Figure 1a**. Poly

(ethylene glycol) diacrylate (PEGDA) was used as a cross-linker, and 2-hydroxy-2-methylpropiophenone (HMPP) as the photo-initiator. The cross-linker concentration was fixed as 1.0 wt.% of the total weight of the monomers/oligomers. The initiator concentration was also kept constant at 1.0 wt.% with respect to the total weight of the monomers and cross-linker in the reactive solution. The reactive mixture in the desired ratio was cast between two polyethylene terephthalate (PET) films and subjected to UV-curing for 15 min. to undergo crosslinking polymerization leading to the polymer electrolyte membranes with solid-like operability and dimensional stability. The membranes formed hence are treated with 6 M KOH + 0.2 M $Zn(OAc)_2$ solution for 24 h to form the OH^--doped polymer membranes herein referred to as the anion exchange polymer electrolyte membranes (AEPEMs).

Further, to prepare the AEPEM-GF, a glass fiber (GF) separator (Whatman GF/F CAT No. 1825-047) was first soaked in a reactive solution of AOETMA:HEMA: PEGMEMA at the ratio of 1.4: 5.6: 3 (w/w %) and then subjected to UV irradiation for 15 min, followed by OH^- doping by soaking in 6 M KOH+ 0.2 M $Zn(OAc)_2$ solution for 24 h. The above-prepared AEPEM (90:10, 70:30 and 50:50) and AEPEM-GF were used for further studies throughout the work.

Zinc-air battery (ZAB) fabrication and testing:

Air-cathode preparation:

The commercial state-of-the-art 40% Pt/C catalyst was procured from Alfa-Aesar and RuO_2 from Sigma Chemicals. The Pt/C-RuO_2 slurry was prepared in isopropyl alcohol, 10% Fumion solution was added, and the mixture was sonicated for 1 h. The Pt/C: RuO_2 ratio was maintained as 1:1. The prepared slurry was brush-coated over a Sigracel GDL and dried in a vacuum oven at 60 °C.

Rechargeable quasi-solid-state ZAB device with the (rZAB (*in-situ*)) and without (rZAB (direct)) the *in-situ* polymerized air-cathode:

The rechargeable quasi-solid-state ZABs were assembled with Zn paste as the anode, the catalyst-coated GDL as the air-cathode, and AEPEM-GF as the quasi-solid-state electrolyte in an electrochemical ZAB set-up (MTI Corporation). ZAB was fabricated by sandwiching the AEPEM-GF between the zinc anode and catalyst-coated GDL. This device is designated as rZAB (direct). To fabricate the device possessing the *in-situ* polymerized air-cathode (rZAB (*in-situ*)), prior to the device fabrication, a thin polymer (AHM) layer was coated over the catalyst-coated air-cathode and subjected to UV irradiation to develop an AHM-skin over the *in-situ* polymerization over the catalyst surface.

Fabrication of flexible, rechargeable ZAB (F-rZAB (*in-situ*)):

For the fabrication of the flexible and rechargeable Zn-air battery (F-rZAB (*in-situ*), a thin Zn foil of 0.1 mm thickness was chosen as the anode. A catalyst-coated carbon cloth (ZOLTEK™ P×30 Fabric PW03/ thickness 406 microns) with a thin layer of the *in-situ* polymerized precursor solution was used as the cathode, and the developed AEPEM-GF was employed as the quasi-solid-state electrolyte. The AEPEM-GF was sandwiched between the modified catalyst-coated carbon cloth and the Zn foil to form a flexible, rechargeable ZAB (F-rZAB (*in-situ*).

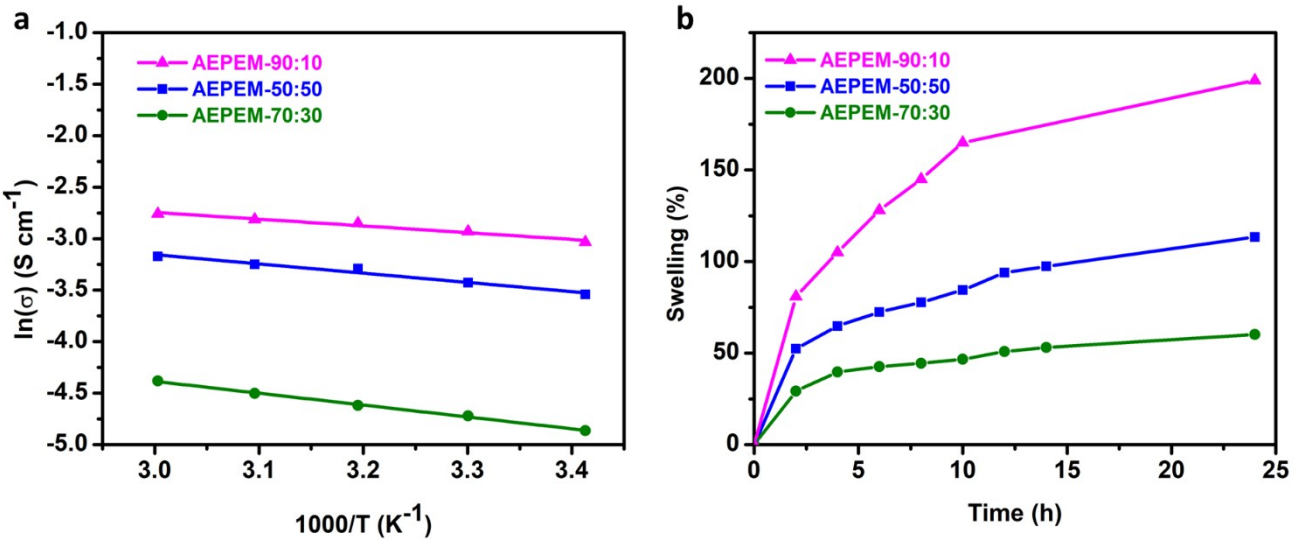

Fig. S1. a) The ionic conductivity *vs*. temperature comparison plots associated with the AEPEM-50:50 and AEPEM-90:10 membranes and b) the electrolyte uptake analysis of the membranes.

Table S1. Table depicting the ionic conductivity of the various membranes prepared.

AEPEM membrane	Ionic conductivity at 30 °C (S cm^{-1})
AEPEM-50:50	$9.87x10^{-3}$
AEPEM-70:30	$3.25x10^{-2}$
AEPEM-90:10	$8.5x10^{-2}$
AEPEM-GF	$9.0x10^{-2}$

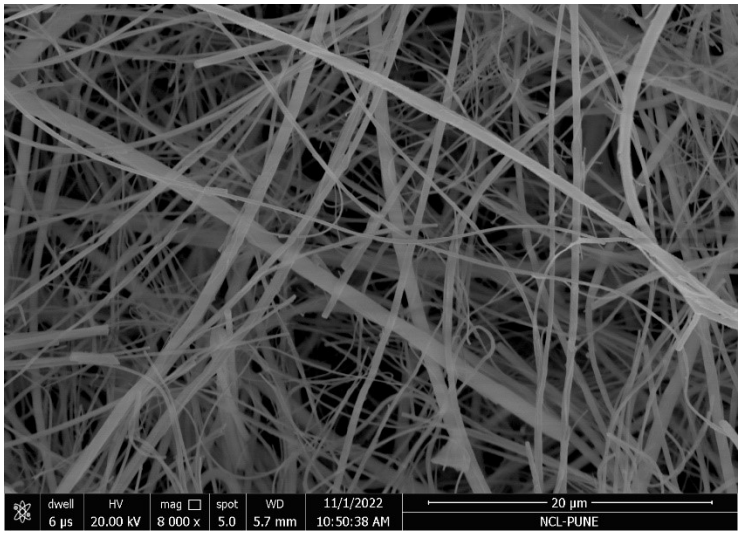

Fig. S2. The FE-SEM image of the glass fiber (GF) paper showing the porous nature of the sample

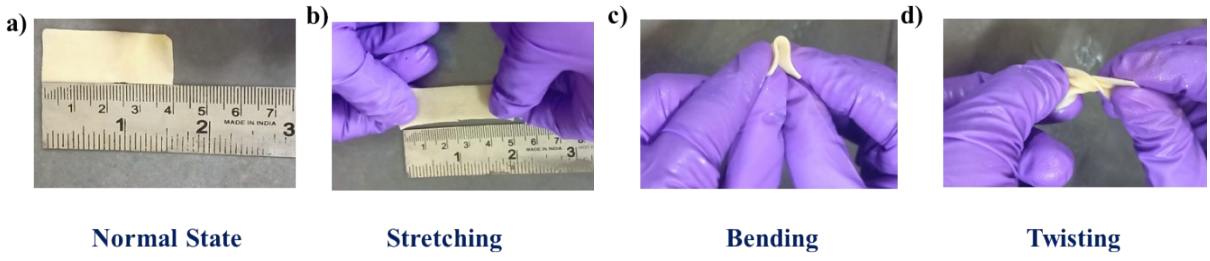

Fig. S3. The photographic images demonstrating the flexibility of the prepared AEPEM-GF membrane.

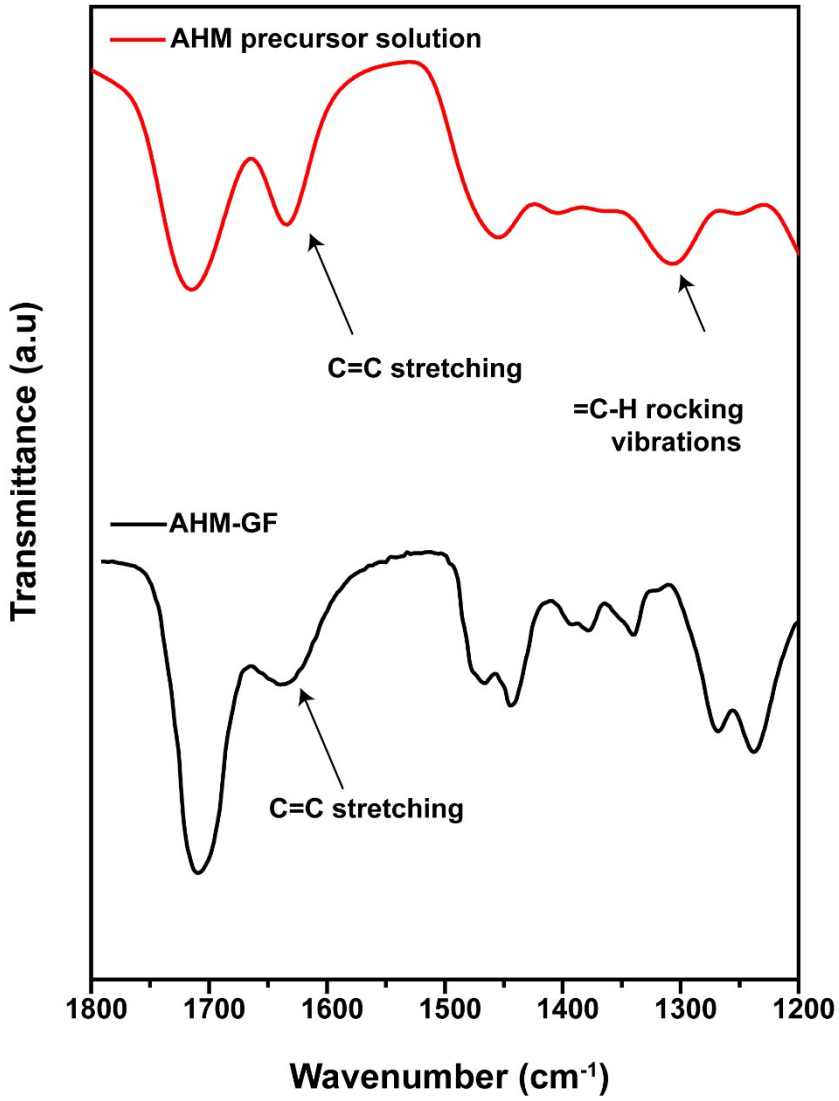

Fig. S4. The ATR-FTIR spectra representing the -C=C- peaks for the precursor solution and the AHM-GF membrane after the UV polymerization.

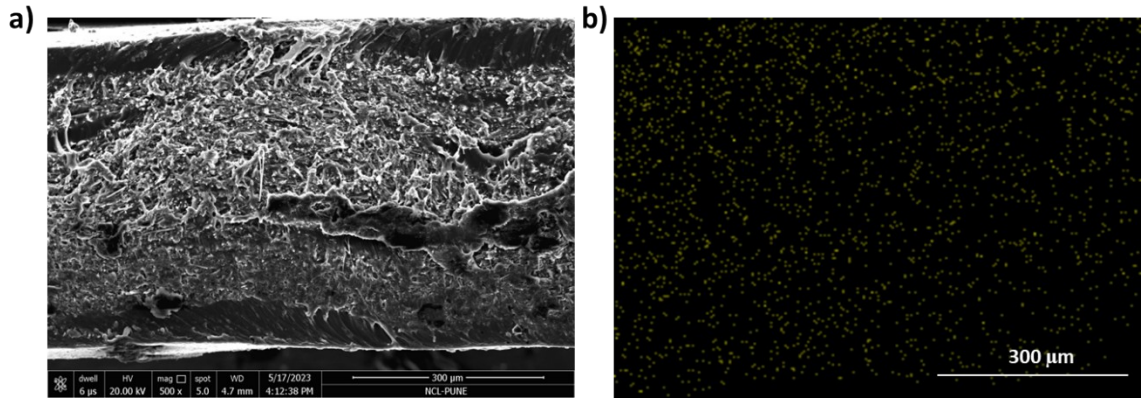

Fig. S5. a) The cross-sectional FESEM image of the AEPEM-GF membrane showing the interconnected network morphology owing to the growth of the polymer over the glass fiber scaffold, b) and the elemental mapping corresponding to Cl, which is present in AOETMA, implying the uniform distribution of the species throughout the membrane thus substantiating the formation of uniform AEPEM over the GF fibers.

Table S2. Properties of the AEPEM-GF membrane compared to the commercial and already reported anion conducting membranes.

Membranes	Temperature	Ionic conductivity (S cm^{-1})	Electrolyte uptake (%)	References
AEPEM-GF	R.T	9.0×10^{-2}	135	This work
Fumasep® FAA 3-30	R.T	4.0×10^{-2}	-	[1]
A201 5	R.T	4.2×10^{-2}	25	[2]
QAFCGO (5)	R.T	3.33×10^{-2}	124	[2]
2-QAFC 6	R.T	2.12×10^{-2}	95	[3]
CS-PDDA-OH 7	R.T	2.4×10^{-2}	159	[4]
a5-QAPS 9	R.T	2.8×10^{-2}	-	[5]
PGG-GP	R.T	12.3×10^{-2}	140	[6]

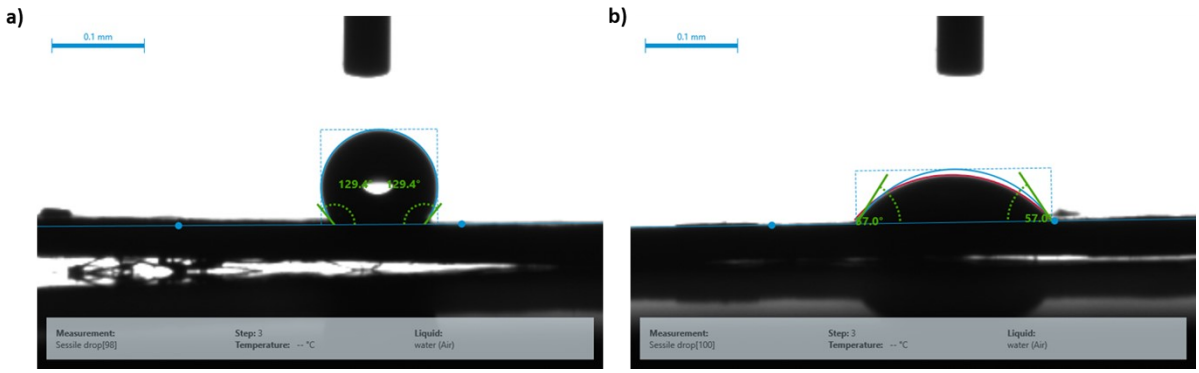

Fig. S6. The contact angle measurements of a) the conventional Pt/C-RuO_2-coated air-electrode, and b the AHM-skin-integrated Pt/C-RuO_2-coated air-electrode.

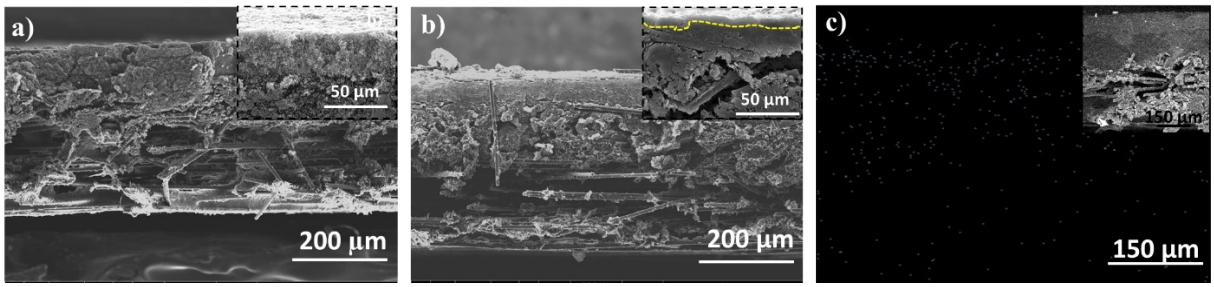

Fig. S7. The cross-sectional FESEM images of a) conventional Pt/C-RuO_2-coated air-electrode, b) AHM-skin-integrated Pt/C-RuO_2-coated air-electrode, and c) the elemental mapping corresponding to Cl, which is present in AOETMA, for the AHM-skin integrated air-cathode, implying the uniform distribution of the species throughout the electrode (inset image shows the mapped area).

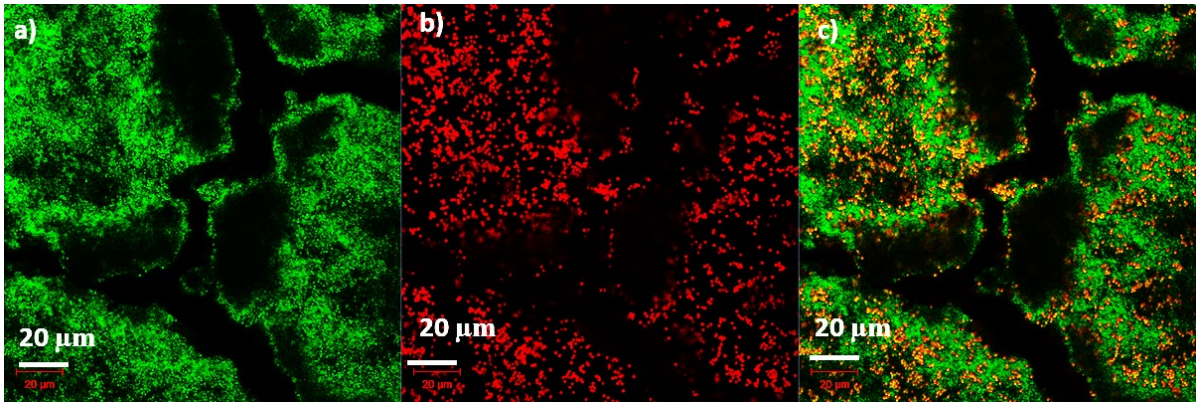

Fig. S8. a) The 2D confocal image for the air-cathode surface obtained under reflection mode, b) the 2D confocal fluorescent image of the dispersed particles (tracers), and c) the 2D overlay image of a and b demonstrating the distribution of fluorescent particles over the air-electrode surface and hence substantiating the polymer coverage.

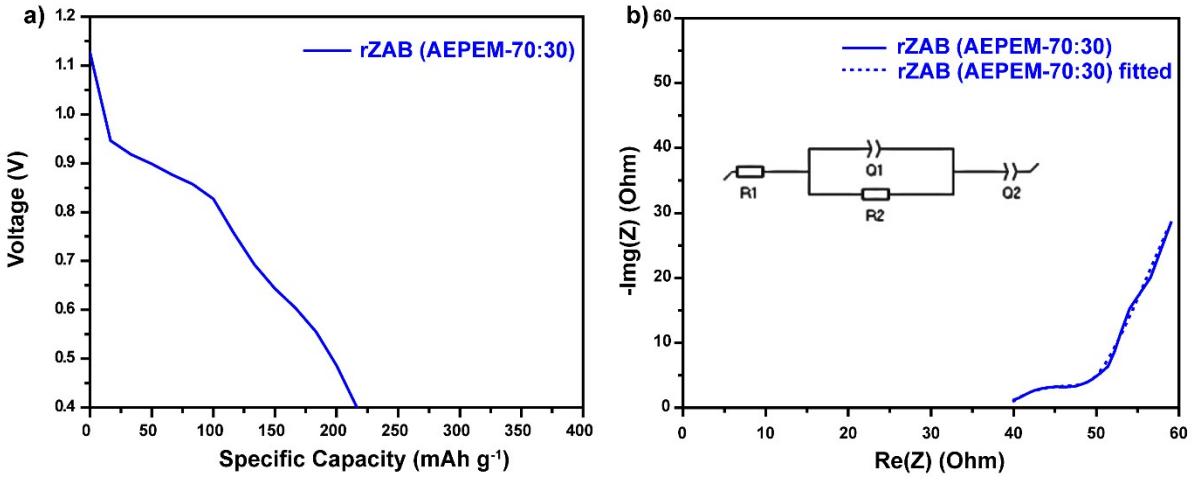

Fig. S9. The ZAB performance analysis of rZAB (AEPEM-70:30): a) the galvanostatic discharge capacity after normalizing with the consumed amount of zinc during the process, and b) the Nyquist plot obtained from the EIS analysis at the OCV condition with the equivalent circuit model fit (inset).

Table S3. The impedance parameters derived from the Nyquist plots of the rZAB (AEPEM-70:30), rZAB (direct) and rZAB (*in-situ*) systems.

Impedance parameters	rZAB (AEPEM-70:30)	rZAB (direct)	rZAB (*in-situ*)
R_0 (Ω)	39.06	6.634	1.652
R_{ct} (Ω)	15.14	11.43	8.005

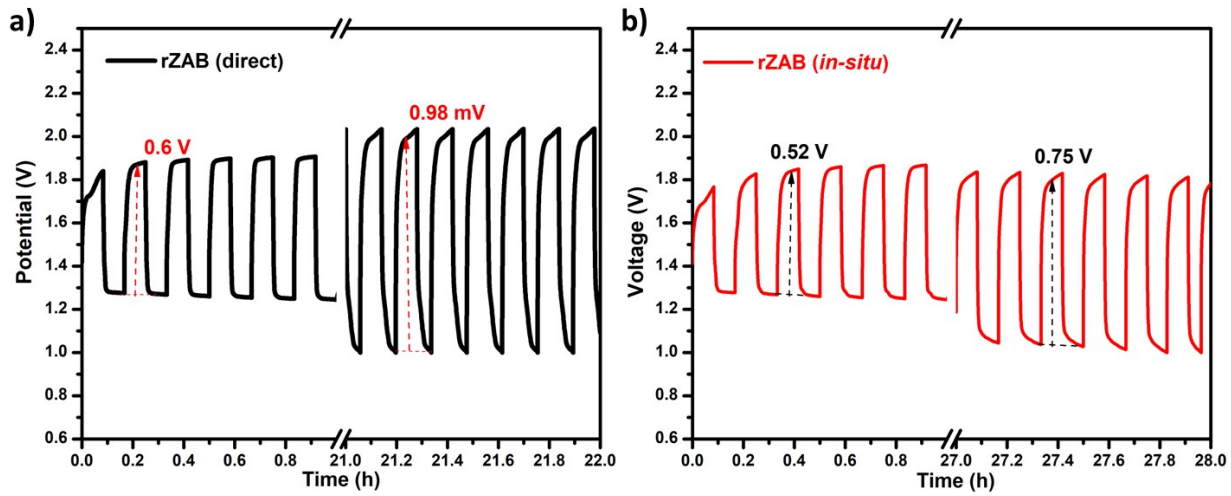

Fig. S10. The charge-discharge plots of a) the rZAB (direct) and b) the rZAB (*in-situ*) showing the overpotential at the initial and final cycles.

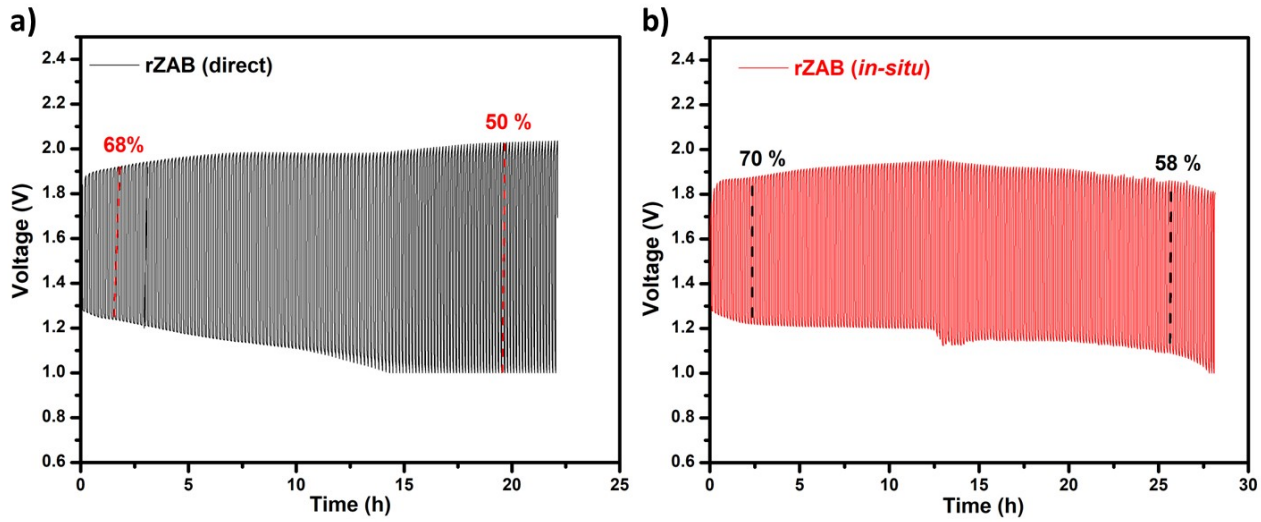

Fig. S11. The charge-discharge plots of a) the rZAB (direct) and b) the rZAB (*in-situ*) systems showing the voltage efficiency at the initial and final cycles.

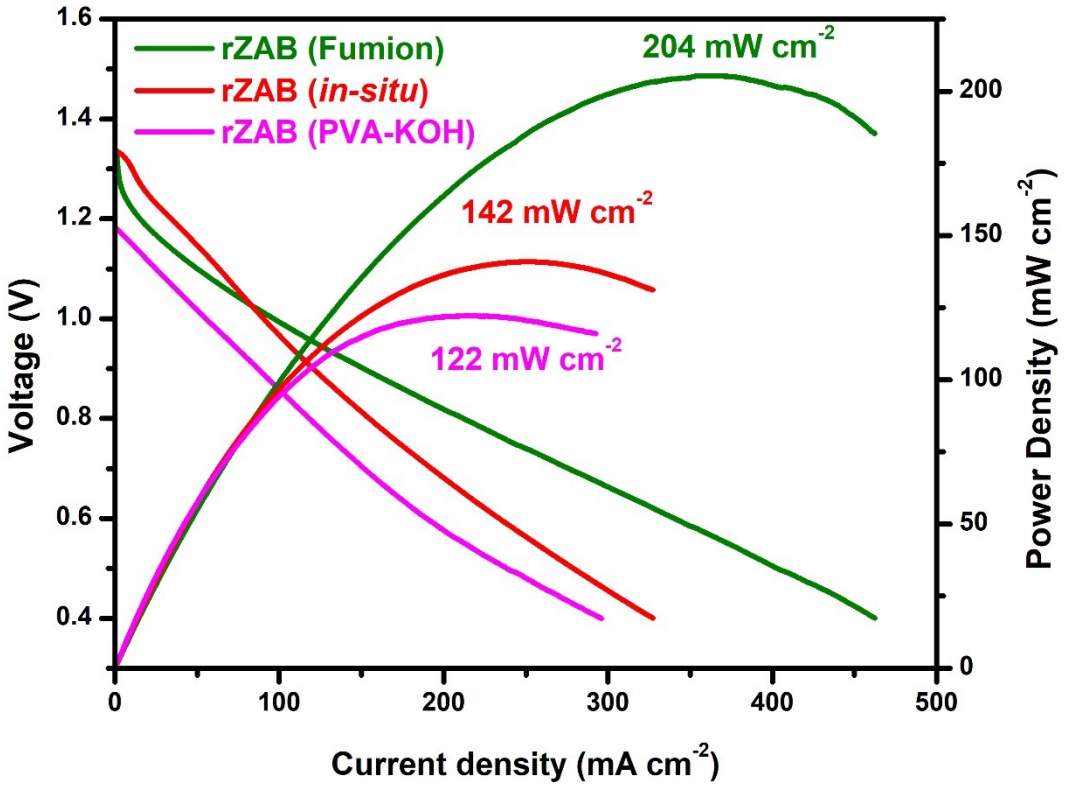

Fig. S12. The solid-state rechargeable zinc-air battery (ZAB) performance evaluation for the rZAB (Fumion), rZAB (*in-situ*) and rZAB (PVA-KOH) systems.

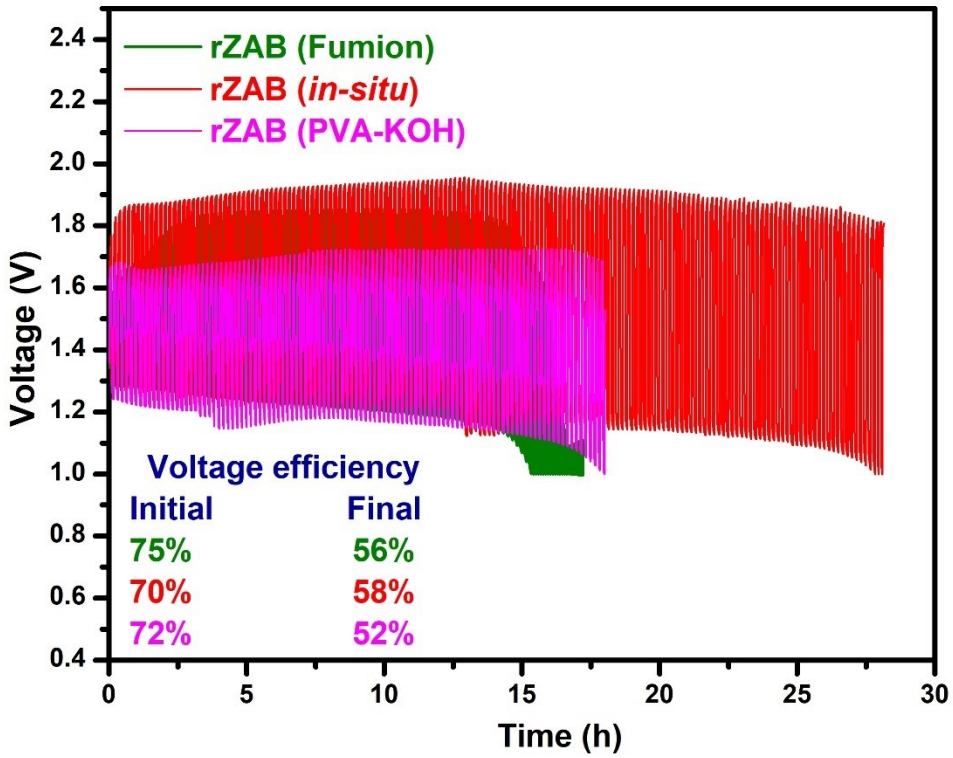

Fig. S13. The charge-discharge comparison plots of the rZAB (Fumion), rZAB (*in-situ*) and rZAB (PVA-KOH) systems.

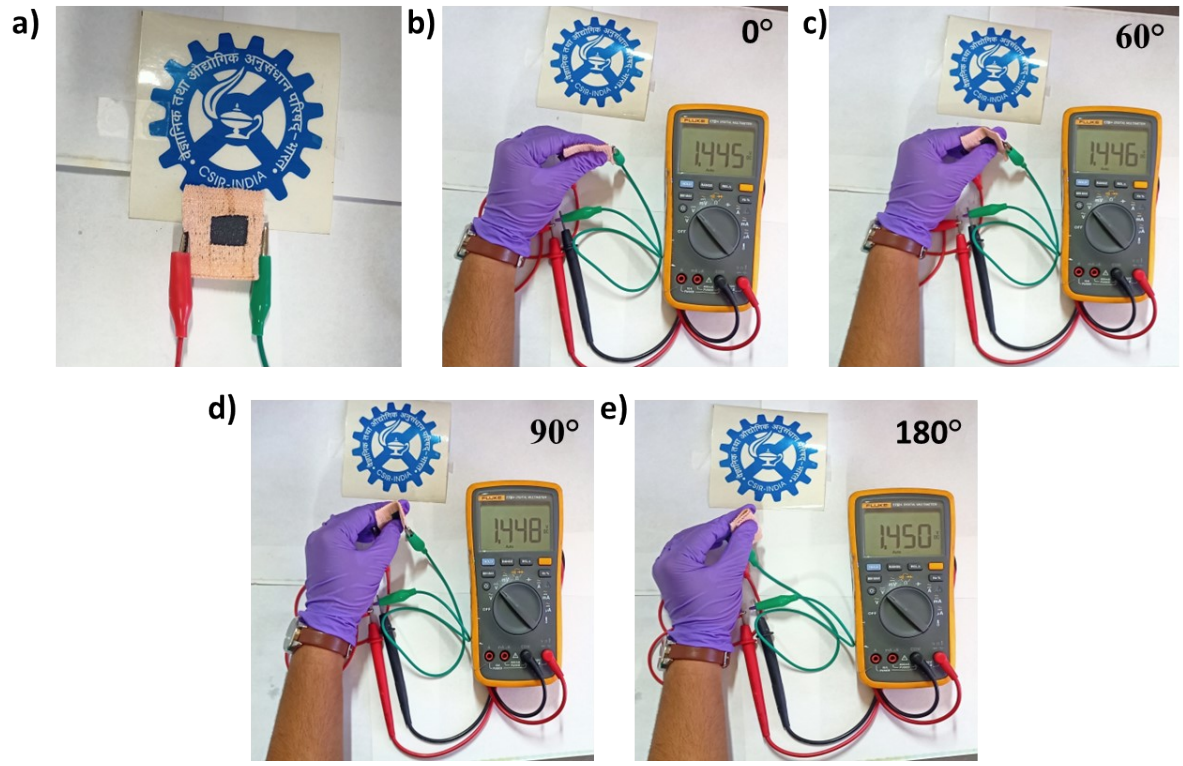

Fig. S14. The photographs of the in-house fabricated flexible zinc-air battery with the demonstration of the output potential of F-rZAB (*in-situ*) at the various bending angles as marked in the image.

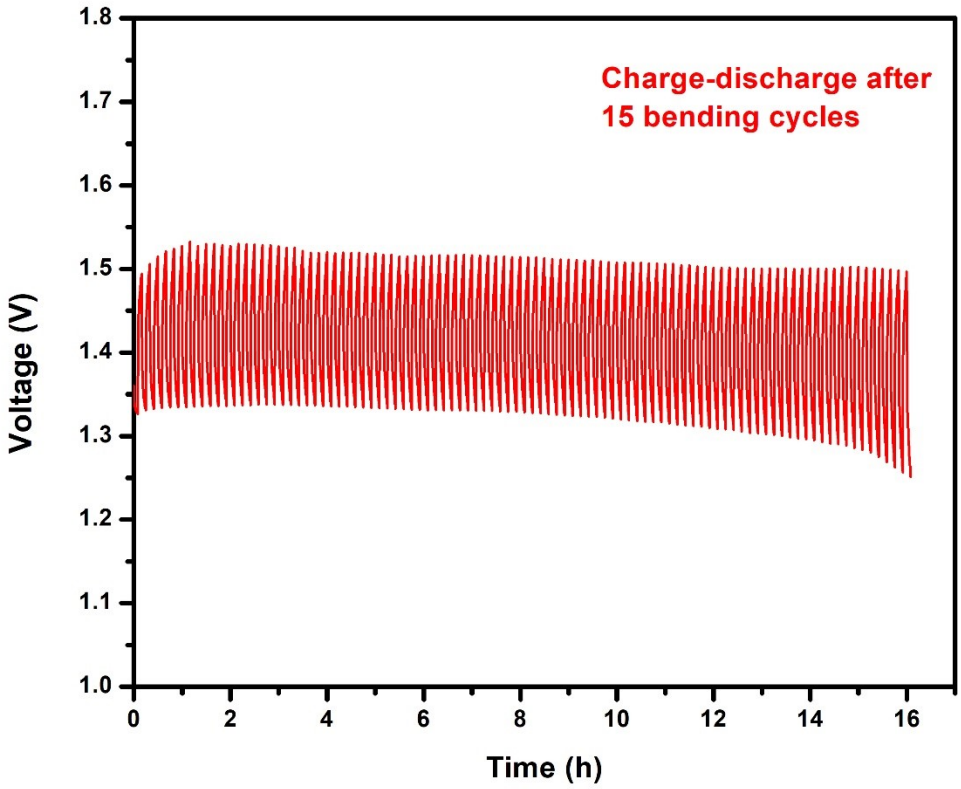

Fig. S15. The charge-discharge plot for F-rZAB after 15 times bending cycles.

Table S4. Comparison of the electrochemical performance of the ZABs based on the current work and those based on the other gel electrolytes reported in the literature.

Electrolyte	Air Electrode	Power density (mW cm^{-2})	Cycling Stability (time per cycle, current density)	Ref.
AEPEM-GF with *in-situ* polymerized cathode	**Pt/C-RuO_2**	**143**	**28 h (10 min, 5 mA cm^{-2})**	**This work**
Polyacrylonitrile (PAN)-based membrane (HPPANP)	Pt/C/ IrO_2	93.6	~20 h (20 min, 10 mA cm^{-2})	[7]
KI–PVAA–GO GPE	Pt/C + Co_3O_4	78.6	200 h (1 h, 2 mA cm^{-2})	[8]
AAEM composed of poly(vinyl alcohol)/guar hydroxypropyltrimonium chloride (PGG-GP)	IrO_2 and 40 wt% Pt/C/carbon cloth	50.2	10 h (10 min, 2 mA cm^{-2})	[6]
Sodium polyacrylate (PAA-Na) hydrogel	MnO_2/C	100.7	183 cycles (10 mA cm^{-2})	[9]

References

1. D. Henkensmeier, M. Najibah, C. Harms, J. Žitka, J. Hnát and K. Bouzek, *Journal of Electrochemical Energy Conversion and Storage*, 2020, **18**.
2. J. Zhang, J. Fu, X. P. Song, G. P. Jiang, H. Zarrin, P. Xu, K. C. Li, A. P. Yu and Z. W. Chen, *Advanced Energy Materals*, 2016, **6**, 1600476.
3. J. Fu, J. Zhang, X. Song, H. Zarrin, X. Tian, J. Qiao, L. Rasen, K. Li and Z. Chen, *Energy & Environmental Science*, 2016, **9**, 663-670.
4. Y. Wei, M. Wang, N. Xu, L. Peng, J. Mao, Q. Gong and J. Qiao, *ACS Appl Mater Interfaces*, 2018, **10**, 29593-29598.
5. J. Han, J. Pan, C. Chen, L. Wei, Y. Wang, Q. Pan, N. Zhao, B. Xie, L. Xiao, J. Lu and L. Zhuang, *ACS Applied Materials & Interfaces*, 2019, **11**, 469-477.
6. M. Wang, N. Xu, J. Fu, Y. Liu and J. J. J. o. M. C. A. Qiao, *Journal of Materials Chemistry A*, 2019, **7**, 11257-11264.
7. W. Peng, Z. Chen, J. Jin, S. Yang, J. Zhang and G. Li, *ACS Applied Materials & Interfaces*, 2022, **14**, 31792-31802.
8. Z. Song, J. Ding, B. Liu, X. Liu, X. Han, Y. Deng, W. Hu and C. Zhong, *Advanced Materials*, 2020, **32**, 1908127.
9. S. Zhao, K. Wang, S. Tang, X. Liu, K. Peng, Y. Xiao and Y. Chen, *Energy Technology*, 2020, **8**, 1901229.